American Mineralogist, Volume 71, pages 85–94, 1986

Kinetics of mineral-water reactions: theory, design and application of circulating hydrothermal equipment

J. Posey-Dowty, David Crerar and Roland Hellmann

Department of Geological and Geophysical Sciences
Princeton University, Princeton, New Jersey 08544

and Clarence D. Chang

Mobil Research and Development Corporation
Princeton, New Jersey 08540

Abstract

A circulating apparatus has been specifically designed for kinetic studies of mineral–water interactions in hydrothermal systems. The equipment can be operated to 350°C and 140 bars with flow rates of 0.5 to 320 mL/hr. It can be used in a variety of modes depending on the application: semi-static, continuously-fed stirred tank reactor (CSTR), plug flow and packed-bed. The theory of operation and derivation of kinetic rate laws in each basic mode is outlined. Experimental examples are presented for the dissolution kinetics of calcite, fluorite and magnetite in simple aqueous systems to 350°C and 140 bars using CSTR, packed-bed plug flow and semi-static modes.

Introduction

Relatively little is known at present about the rates and chemical mechanisms of mineral reactions in hydrothermal solutions. Previous high-temperature studies on the dissolution kinetics of feldspar by Lagache (1976) and of silica by Rimstidt and Barnes (1980) have used conventional static equipment; in that approach, fluid samples are withdrawn periodically from a sealed autoclave, and rate laws are determined from the change in concentration with time. Rimstidt and Barnes (1980) have also used a semi-batch reactor similar to the one discussed below.

The present paper describes a hydrothermal apparatus which greatly facilitates kinetic studies at temperatures and pressures up to 350°C and 140 bars. This equipment can be operated as a conventional static system, but in addition can be run in a variety of circulating modes. When used as a circulating system, rate laws are determined from steady-state rather than time-dependent concentrations. A major advantage is the ability to vary the chemistry of the input stream over the course of an experiment; this simplifies and greatly reduces the number of experiments required to determine reaction orders and other rate parameters.

Flow system design

Flow reactors of widely varying design are often used in engineering and industrial processes (e.g., Bunn, 1976; Carberry, 1976; Levenspiel, 1972). The apparatus described in this paper has been designed specifically to study the kinetics of hydrothermal mineral–water interactions and other solid–liquid or solid–gas systems at the laboratory scale. There has been some previous geochemical work on mineral solubilities using flow reactors (Morey and Hesselgesser, 1951; Sweeton and Baes, 1970; Kanert et al., 1978; Tremaine and LeBlanc, 1980). However, it is difficult to demonstrate chemical equilibrium in such experiments, and these flow systems by their very nature are better suited for kinetic studies.

The general design of the flow system is outlined in Figure 1. For our particular purposes, we have used tubular autoclaves or reaction vessels constructed from 316 stainless steel, pure titanium, or other corrosion-resistant alloys, with internal volumes ranging from tens to hundreds of milliliters. These vessels are fitted with either standard coned ¼″, taper-seal ⅛″ or 1/16″ inlet and outlet ports at opposite ends. For particularly corrosive applications, the vessels can be lined with inert materials such as teflon, titanium, or gold. By changing the aspect ratio (a length to diameter ratio), the flow apparatus can usually be operated between two ideal flow regimes, plug flow and well-mixed flow. System pressure is maintained and controlled up to 140±0.68 bars by a gas-loaded back pressure regulator with a teflon diaphragm (Grove Model S-91XW), located on the outlet side of the vessel. Located on the input side are two separate pumps, each with its own set of safety rupture disks and one-way valves (HIP, Inc.; parts 60-61HF4 and 15-41AF2-T, respectively). Fluids are continuously pumped through the autoclave at flow rates from 0.5 to 320 mL/hr by an HPLC pump (either a Milton Roy Model 396 minipump or an Isco Model 314). The second liquid pump (Haskell Model MCP-71), rapidly replaces large volumes of liquid and is used to initially charge the system, or to replace solution withdrawn by sampling in the semi-static mode.

Gas mixtures can be fed into the input stream at precisely controlled rates using an electronic mass flow meter (Porter Instrument Company, Inc.; Model F221), with a flow rating of 0–5 cc/min. Mixtures of gases (such as hydrogen or carbon dioxide with an inert gas) can be used to control the gaseous fugacities

0003–004X/86/0102–0085$02.00

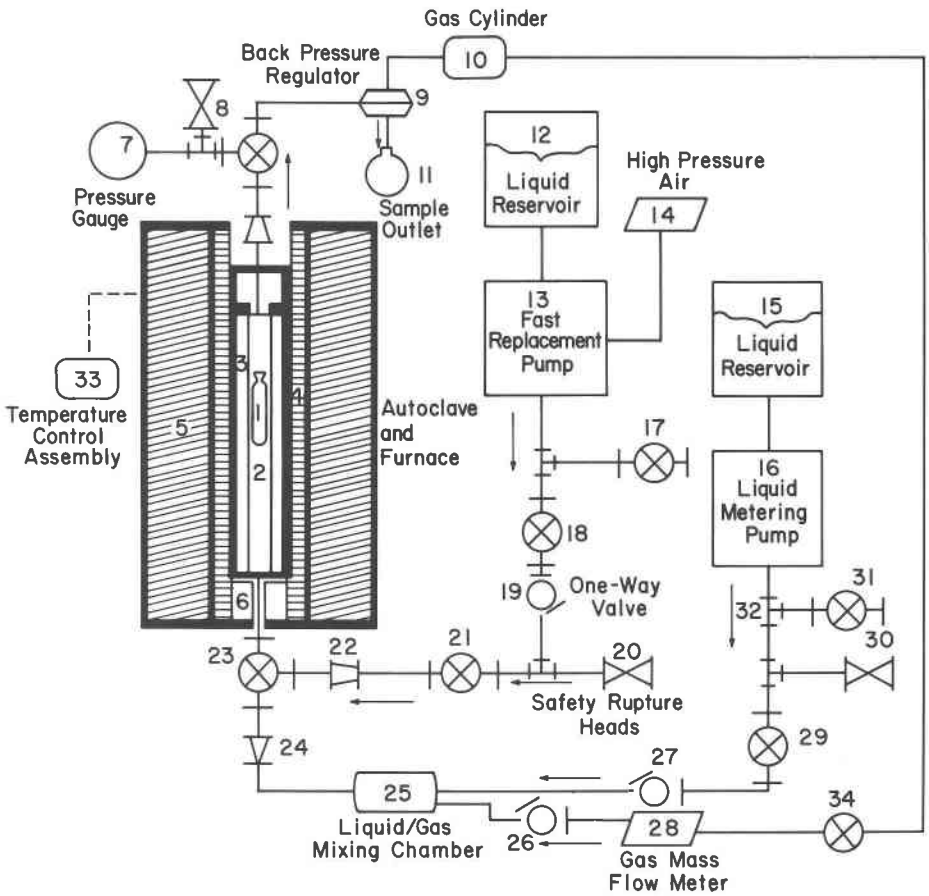

Fig. 1. Schematic diagram of circulating hydrothermal equipment with controlled liquid and gas inputs, operable to 350°C, 140 bars. 1 = sample and holder, 2 = gold mesh support tube, 3 = reaction vessel, 4 = furnace, 5 = insulation, 6 = lavalite support block, 7 = pressure gauge, 8 = valve, 9 = back pressure regulator, 10 = gas cylinder, 11 = sample outlet, 12 = liquid reservoir, 13 = fast acting liquid replacement pump (Haskell gas loaded-diaphram liquid stroke minipump), 14 = high pressure air, 15 = liquid reservoir, 16 = liquid metering pump (Isco or Milton Roy minipump), 17 = valve, 18 = valve, 19 = one-way valve, 20 = safety rupture head, 21 = valve, 22 = reducer, 23 = valve, 24 = reducer, 25 = liquid and gas mixing chamber, 26 = one-way valve, 27 = one-way valve, 28 = mass flowmeter, 29 = valve, 30 = safety rupture head, 31 = valve, 32 = tee, 33 = temperature control assembly, 34 = gas regulator and valve.

in the hydrothermal solution. Liquid and gas are input to a preliminary mixing chamber consisting of a vertically-mounted stainless steel autoclave with two one-way inlets (one liquid and one gas inlet) and a single outlet for the mixture. In order for the metering method to work properly, pressure at the inlet port must be slightly higher than at the back pressure regulator. This is accomplished by bleeding off a small volume of gas at the back pressure regulator just before turning on the gas metering system. The Isco pump (unlike the Milton Roy HPLC pump) allows gas-saturated solutions to be input at system pressure, without vapor locks, but must be recharged after each 350 mL stroke of the piston. The autoclaves are heated by conventional furnaces, which are adjusted to minimize longitudinal temperature gradients. The temperature is set by time-proportioning controllers which trigger mercury relays; the electrical power is adjusted with variable transformers.

Theory of flow operation

Depending on the properties of the fluid and the configuration of the reaction vessel and sample, the above apparatus can be operated in different modes: (1) Semi-static (semi-batch) with easy input and output of solution; (2) well-mixed continuous flow reactor (or continuously-fed stirred tank reactor, CSTR); and (3) plug flow reactor. Experiments involving mineral–water reactions and heterogeneous catalysis often use reactors with packed-beds, where experimental conditions (packing, permeability, porosity, flow rate, reactor aspect ratio, etc.) determine the flow regime occurring within the reactor. This versatility is an important advantage because it is possible to choose the optimal mode for a particular reaction or process without redesigning or significantly rebuilding the apparatus. We have successfully tested and used all solid–liquid modes and present the theory of operation and typical results below.

We should emphasize at the outset the importance of choosing the correct reactor model. An incorrect interpretation of parameters, such as diffusion (e.g., eddy and

molecular), mass and heat transfer, the effect of gradients, etc., can lead to incorrect modelling and errors of one or two orders of magnitude in the derived rate constants—see an example given by Poirier and Carr (1971). The theory of reactor models is discussed at length by Levenspiel (1972), Carberry (1960), Johnson and Huang (1956), Sherwood et al. (1975), and others.

Semi-static or batch reactors

In conventional static reactors, samples are withdrawn periodically from an otherwise closed system, and changes in concentration are measured as a function of time. In pressurized, high-temperature systems, fluid pressure and density necessarily drop with each sampling if the vessel is filled with fluid alone. With vapor and fluid present, pressure remains fixed, but the ratio of fluid to solid reactants decreases with each sampling. Such experiments are ultimately limited by the amount of solution that can be withdrawn before emptying the vessel.

The above difficulties can be circumvented by replacing withdrawn fluid with fresh solution at each sampling. This is accomplished in the apparatus described above by the fast-acting pump (#13) illustrated in Figure 1. The fast acting pump is set to self-activate at a pressure slightly higher than the back pressure regulator. Therefore, opening and closing valve #18 (Fig. 1) forces solution through the vessel and out the back pressure regulator where the sample is collected. During this mode of operation, valve #29 remains closed. We define such systems in which fluid is both periodically withdrawn and simultaneously replaced as semi-static reactors.

Using the algorithm outlined in the Appendix to this paper, it is possible to correct for the dilution caused by addition of fresh solution at each sampling. The corrected data can then be analyzed as in a batch reactor. Theoretical rate laws are integrated and then fitted to the data to determine which expression yields the best fit. This provides both the order of reaction and the rate constant for simple reactions. For a list of integrated rate equations, see Laidler (1965, p. 7ff).

In some mineral–water systems, reaction rates are sufficiently slow that the initial parameters do not change extensively throughout the course of an experiment. The method of initial rates can then be used to determine the rate laws and reaction orders with respect to specific variables far from equilibrium (Lasaga and Kirkpatrick, 1981; Chapter 1). With these same minerals, diffusion and transport is approximately two to four orders of magnitude faster than the rate of reaction, so that the terms describing transport at the solid-solution interface can be neglected (Carberry, 1976). Other minerals, whose reaction rates in solution are rapid must be corrected for diffusion and transport.

Packed-bed reactor

As mentioned earlier, solid–liquid reactions are frequently carried out in tubular reactors with the solid reactant packed or suspended in the tube and the liquid passed through it during the course of a reaction. The general equation for any reaction carried out in a flow tube, assuming bulk flow in the axial direction and radial symmetry, is:

$$\underset{a}{\frac{1}{V}\frac{\delta V[C]}{\delta t}} + \underset{b}{\frac{\delta A_z\, u[C]}{A_z\, \delta z}} - \underset{c}{D_a \frac{\delta^2[C]}{\delta z^2}} - \underset{d}{\frac{D_r}{r} r \frac{\delta}{\delta r}\left(r \frac{\delta[C]}{\delta r}\right)} = \underset{e}{R_c} + \underset{f}{R_t} \qquad (1)$$

In cylindrical coordinates, r is the radial direction and z is the axial direction. D_a is the axial dispersion coefficient; D_r is the radial dispersion coefficient; R_c is the homogeneous rate of reaction; R_t is the heterogeneous rate of reaction, including mass transport of material to and away from the surface of the solid; Term a in equation (1) is the bulk mass rate of flow of [C] (molarity) in the tube; u is the average linear velocity in the z-direction and V is the volume of liquid in the void space in the reactor (Carberry, 1976).

Unfortunately, there is no general analytical solution to Equation 1. Therefore, the importance of each of the parameters must be evaluated approximately both experimentally and theoretically; one of three general approximate methods then used to solve the equation: (1) If the axial dispersion is sufficiently large (as it is in a stirred tank), the reactor is considered to be a CSTR. The equations to evaluate reaction kinetics in CSTR's are discussed in a following section. (2) If the axial dispersion is small on the other hand, the reactor is usually considered to be a plug flow reactor. (3) If intermediate conditions exist, the size and shape of the reactor is changed so that either (1) or (2) is used. Otherwise, a complex mathematical solution to the differential equation must be sought. The interphase mass transport term and mass transport of the dissolving solid are considered separately.

Transport between the bulk solution and the surface of the solid must be estimated in any case. Transport coefficents depend on concentration gradients and fluid flow in the reactors and are calculated from literature tabulations of experimental coefficients of transport. Some simple empirical equations in order to do this are given below.

For isothermal packed-bed reactors the principle design elements to be considered in context of the present application are fluid dynamics and fluid-particle mass transfer. Dispersion in packed-beds is usually characterized by the radial and axial Peclet numbers, Pe_r and Pe_a. For liquid water at flow rates under similar conditions to our studies (unagitated flow), these numbers have the approximate ranges:

$$Pe_r = (ud)/D_r = 8\text{–}50 \qquad (2)$$

$$Pe_a = (ud)/D_a = 0.1\text{–}2 \qquad (3)$$

u is an average linear velocity; d is the effective particle diameter; and D_r, D_a are apparent radial and axial diffusion coefficients, which should be determined experi-

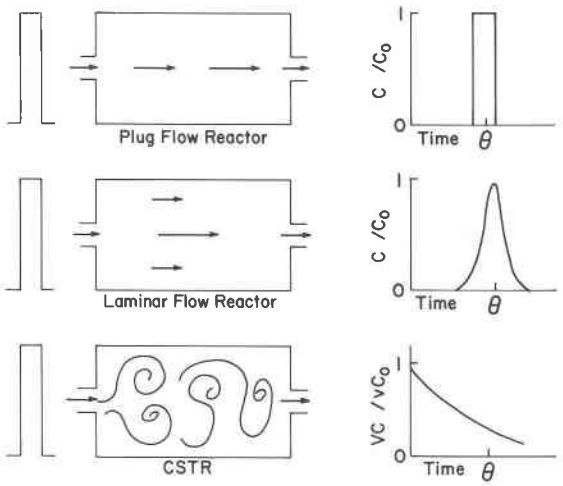

Fig. 2. Ideal behavior of inert chemical tracer spikes in (A) plug flow, (B) laminar flow and (C) CSTR reactors. Left hand figures illustrate input of sharply defined tracer spike. Middle figures show the rough distribution of tracer within each reactor. Right hand figures plot concentration of tracer in output stream vs. time (expressed as fluid residence time, Θ).

mentally also. A helpful figure compiling experimental values of axial and radial dispersion coefficients as a function of Reynold's number is found in Sherwood, Pigford and Wilke (1975), for example. Radial nonuniformity is usually negligible since D_a is normally larger than the molecular diffusion coefficient. The effects of axial dispersion can be eliminated by careful attention to bed geometry, specifically the length-to-diameter aspect ratio. A useful criterion in this regard has been developed by Zahner (1972). It is quite useful to compare these calculated dispersion parameters to experimental ones, derived from tracer studies.

Knowledge of the non-ideality of a flow system is imperative for the proper formulation of the kinetic rate law of interest. Experimental tracer studies are commonly employed to determine the degree of non-ideality as a function of the axial and radial dispersion present for a flow system operating under typical experimental conditions. The axial dispersion parameter, which is usually more significant than the radial dispersion parameter, is commonly determined through the introduction of a tracer spike (Dirac δ-function) into the input stream or through a step change in the input chemistry of the liquid reservoir. Figures 2a and 2b demonstrate the behavior of an inert tracer spike for perfect plug-flow and laminar-flow reactors, respectively; Figure 2c is for a CSTR. The general dispersion equation (equation 1) can be used to mathematically formulate the basis of these dispersion measurement techniques. For the case of a tracer injection, an expression incorporating the Dirac δ-function is set equal to R_t (in this case a source term) in equation 1 and the homogeneous reaction term R_c drops out. For a detailed review of various dispersion models and procedures for analyzing experimental tracer data, the reader is referred to the engineering literature, such as Levenspiel and Bischoff (1963).

When experimental and theoretical dispersion coefficients differ significantly, special caution must be used. We find it helpful to construct a cylindrical glass tube having the same dimensions, packing, and fittings as our reactor and into which a dye tracer is admitted. The flow patterns and irregularities as well as bypassing can then be readily seen and the packing and other conditions optimized. Fluid bypassing the solids by flowing close to the wall and then mixing in a small volume just prior to exiting can appear to have a uniform concentration throughout the vessel if only the output is observed. This might, for example, lead to the improper choice of a CSTR model when a plug flow model is more appropriate.

The mass transport in solid–liquid systems is calculated based on the assumption that the flow is either turbulent or laminar. Interphase mass transfer in packed-beds is often characterized by correlations of the form:

$$Sh = j_D ReSc^{1/3} \quad (4)$$

where the dimensionless groups are the Sherwood, Reynolds, and Schmidt numbers respectively, and j_D is the Clinton–Colburn factor. j_D and Sc permit an estimation of the mass transfer coefficient, k_e. For example, for liquids at low Re (laminar flow with $0.0016 < Re < 55$)

$$j_D = (k_e \rho_F y_F / Q) Sc^{2/3} \quad (5)$$

where y_F is a dimensionless mole fraction factor; Q is the mass velocity; and ρ_F is the density of the fluid (Wilson and Geankoplis, 1966). Similar equations are used to determine the mass transport in turbulent fluid flow (e.g., Sherwood, Pigford and Wilke, 1975).

Plug-flow reactors

Plug flow reactors are simple to model mathematically. When operating in the plug flow regime without density change due to the temperature or the reaction, the residence time, Θ, of an entering packet of fluid is simply the effective reactor volume, V, divided by the volumetric flow rate of the entering fluid, q. At 25°C,

$$\Theta = V/q \quad (6)$$

However, in hydrothermal experiments or when using organic solvents (in which the density changes dramatically with temperature or salinity, for example) the residence time is better expressed in terms of mass flow and the mass contained in the reaction vessel, not the volume of the vessel. For pure water:

$$\Theta(T, q) = (\rho_T / \rho_{25°C}) V/q(25°C) \quad (7)$$

where ρ designates the solvent density at temperature T and 25°C, respectively. If the density of the solution changes because of chemical reaction in the vessel, other corrections must be used—see Hill (1977), for example. For simplicity, the examples in the experimental illustrations do not exhibit a density change with reaction. The concentration, [C], in hydrothermal reactions should be ex-

pressed in terms of molality, not molarity. Steady-state concentrations are measured as a function of residence time, Θ (or mass flow rate, Q). The integrated form of the rate equation is then used with residence time data to determine the reaction order and rate constants, as with real time data in static systems neglecting terms a, c, d, of Equation 1, which represent the terms for non-steady-state, axial and radial dispersion in the tube, respectively.

$$\delta[C]/\delta\Theta = R_c + R_t \quad (8)$$

where R_c and R_t are defined in Equation 1. In the case in which there is no competing homogeneous reaction, $R_c = 0$. The flow rate can be adjusted to suit the particular nature of the reaction, optimizing the steady-state concentration of a particular species of interest.

The theoretical amount of dispersion and mass transfer should be calculated, and incorporated into the models where appropriate. As mentioned previously, Sherwood, Reynolds, Peclet, and Schmidt numbers are useful indicators of these quantities and are easily calculated—see for example, Levenspiel (1972).

For heterogeneous mineral–water reactions in which there is rapid transport of water to the surface and fluid away from the surface, the rate of reaction in a plug flow reactor for a simple crystal CX dissolving as ionic species may have the following form:

$$M\delta[C]/\delta\Theta = k_1S_a([A]^a[B]^b \ldots) + k_2S_a(K_e - [C][X]) \quad (9)$$

where $M\delta[C]/\delta\Theta$ represents the differential change in total moles of dissolved solute with respect to residence time; [C] is the concentration of one of the products of dissolution; [A], [B] . . . are other species in solution on which the rate of change depends; S_a is the total surface area of the mineral and k_1 and k_2 are rate constants and K_e is the solubility product under those conditions. The surface area term could be written as a function of dislocation density for the mineral, the crystal habit, trace elements, Θ (if the effective surface area of the particle(s) grows or shrinks), or other parameters. Because the magnitude of the dependence upon these properties requires modelling and analytical techniques not possible at this time, only the bulk surface area is normally included. Hence, there may be a large variation in the rate constants for the dissolution of different specimens of the same mineral. Similarly, for a reaction in which there is slow transport of either reactants to or products away from the solid–liquid interface, the rate equation has the form, if the transport of C is the rate determining step:

$$\delta[C]/\delta\Theta = k'k_eS_a(C' - [C])/M \ldots \quad (10)$$

where C′ is the concentration of C at the surface and [C] is the concentration measured in the bulk solution; k_e is the mass transfer coefficient; k′ is a proportionality constant; and S_a is the total surface area of the crystals. Note: When transport is fast relative to reaction the surface concentration C′ is approximately equal to the bulk concentration and the reaction rate depends solely on the chemical reaction rate at the surface. Unfortunately, there is no general equation for the case when chemical reaction rate at the surface and transport of the products away from the surface are competitive rate controlling mechanisms. Intuitively, the measured rate in this case appears to be smaller than the true value. In the 1930's, the "quasi-stationary method" or "method of uniformly accessible surface" was developed to simplify the problem (Frank-Kamenetskii, 1955). In this theory, the rate of reaction at the surface $dC'/dt \simeq$ rate of transport at the surface, $k_eS_a(C' - [C])/M$. When there is a gradient between the surface and the bulk solution, $C' \neq [C]$, the rate of reaction measured in the bulk solution, $d[C]/d\Theta$ is not equal to the rate of dissolution at the surface (rate of reaction at the surface), $\delta C'/\delta\Theta$.

For example, assume the true rate of reaction for CX dissolving is:

$$dC'/dt = k_1S_a(K_e - C'^2)/M \quad (15)$$

where [C] = [X], C′ = X′ which are the concentrations of species C and X in the bulk solution and at the surface, respectively. Assume transport can be given by:

$$dC'/dt = k_eS_a(C' - [C])/M \quad (16)$$

Using the method of uniformly accessible surfaces, Equations 15 and 16 are set equal and then solved for C′ in terms of [C]. In this case,

$$C' = (-k_e/k_1 + ((k_e/k_1)^2 + 4K_e + 4k_e[C]/k_1)^{0.5})/2 \quad (17)$$

This expression is substituted back into Equations 8 and 15, integrated and solved for the constants:

$$M\delta[C]/\delta\Theta = k_1S_a(K_e - (-k_e/2k_1 + 0.5((k_e/k_1)^2 + 4K_e + 4k_e[C]/k_1)^{0.5})^2) \quad (18)$$

Well-mixed continuous-flow reactors

In this third mode of operation (CSTR), using a vessel with a low aspect ratio, well-mixed flow behavior is found. In this case, fluid components admitted to the vessel are uniformly mixed in the reaction chamber and experience a wide distribution of residence times. The measured output of an inert tracer spike will typically decay as shown in Figure 2c. At steady-state, it is possible to write equations describing flow and reaction in CSTR's which need not be integrated—see Denbigh (1944) and Denbigh et al. (1947) for further details. In general, with rapid transport at the solid–liquid interface, the mass balance condition at steady-state must be for dissolution:

Product Flow Out = Product Flow In + Product Added Due to Reaction

or:

$$Q[C] = Q[C]_o + M(\text{Rate of Reaction}) \quad (19)$$

where Q is the mass flow rate, M is the mass of liquid contained in the vessel, C_o is the initial molal concentration, d[C]/dt is the rate of addition or consumption of [C] by reaction, and [C] is the steady-state output concentration (which is also an average concentration in a

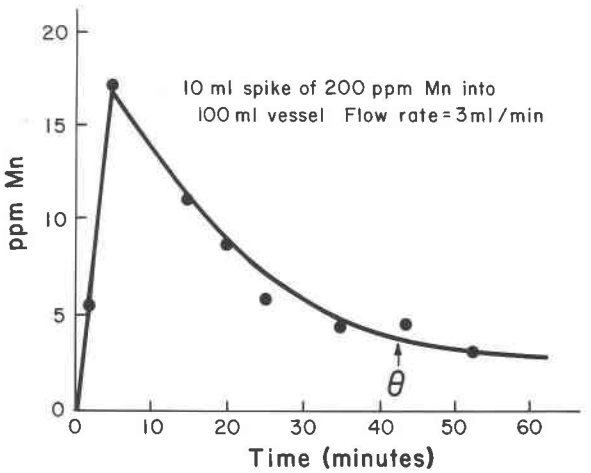

Fig. 3. Concentration of an inert tracer spike in the output stream of the CSTR reactor used for calcite and fluorite dissolution experiments. The position of the residence time, Θ, along the abscissa is noted.

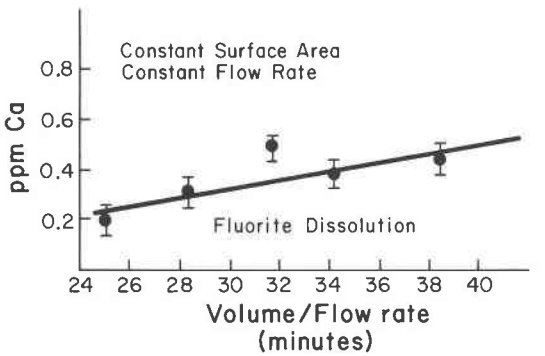

Fig. 4. Steady-state output concentration of total dissolved calcium vs. fluid residence time in a CSTR reactor for fluorite dissolution in water at 75°C.

CSTR). Assuming the average residence time in a CSTR is $\Theta = M/Q$, for CX dissolving in pure water ($[C]_o = 0$), the CSTR equation is similar to the plug flow equation for the same reaction (4). However, the CSTR equation is not integrated:

$$M[C]/\Theta = k_1 S_a([B]^b[D]^d \ldots) + k_2 S_a(K_s - [C][X]) \qquad (20)$$

An example of data we have collected in a packed-bed CSTR with a large liquid/solid ratio and a small liquid/solid ratio is given and discussed below. Mass transport between the bulk phase and the solid surface is handled as described previously using equations 15 and 19 for CSTR's and not integrated rather than using equations 15 and 8 for the plug flow case.

Experimental examples

The application of our flow apparatus can be illustrated with examples from some preliminary experiments on the dissolution kinetics of fluorite, calcite and magnetite in pure water at temperatures and pressures to 350°C and 136 bars, respectively, and with an example of catalysis in a packed bed. These results illustrate both well-mixed flow behavior (CSTR) and plug flow behavior.

The first example is drawn from some preliminary kinetic studies on the dissolution of fluorite and calcite in pure water at high water/mineral ratios. Natural specimens (cleavage fragments or crystals) of either calcite or fluorite were sorted by size and analyzed for trace impurities. The total surface areas were much smaller than could be measured by BET absorption isotherms and therefore had to be calculated by geometrical methods. These crystals were carefully rinsed in an ultrasonic cleaner and examined by SEM to ensure that no particulate fines were present. Crystals (diameter $\gg$ 3 mm) of either mineral were then placed inside a large mesh basket of inconel (mesh size 220). The basket was further supported by a very coarse gold mesh tube suspended inside a 316 stainless steel tubular reaction vessel (internal volume, 100 mL, length, 23 cm, weight of the crystals, 3 g, outlet port, 0.5 cm). The entire flow system was then filled with degassed, distilled water using the fast acting pump, pressurized to the desired setting using the back pressure regulator, and then heated to the first temperature. Flow experiments were initiated by turning on the Milton Roy circulating mini-pump. Water flowed from bottom to top of the vessel, promoting mixing. The gas-mixing apparatus could then be used to regulate the CO_2 and O_2 fugacities.

A 10 mL spike of 200 ppm manganese nitrate tracer was injected either with the fast-acting pump or by a syringe directly into the plastic tubing on the inlet port of the circulating pump to test for flow conditions; similar tests were conducted by step inputs. Although the Reynolds number for this system (0.001–2.0) indicates there should be little turbulence, the results of the tracer spike, shown in Figure 3, indicate the system behaves as a CSTR in this configuration—compare Figure 2c. Combined effects of the liquid flowing from bottom to top, the sample holder, the small inlet and outlet tubing to vessel diameter, the hysteresis in the pump and the thermal gradient at the interface of the relatively cold input fluid and the hot fluid in the vessel, probably all contributed to mixing. The degree of mixing was checked qualitatively by using a dye tracer in a glass tube with the same packing and dimensions.

Steady-state concentrations are reached after a period equivalent to approximately three times the average residence time, 3Θ. When changing flow conditions, it is important to allow at least 3Θ between successive samplings to enable a steady state to be reached. Steady-state concentrations are measured at each temperature as a function of flow rate (or residence time). Typical results for fluorite dissolving in pure water at 75°C are shown in Figure 4. The linearity of this plot indicates that fluorite dissolution is pseudo-zero order with respect to products far from saturation, and follows the law $d[Ca]/dt = k$, or in this case, $[Ca] = k\Theta$ (from equation 20 above).

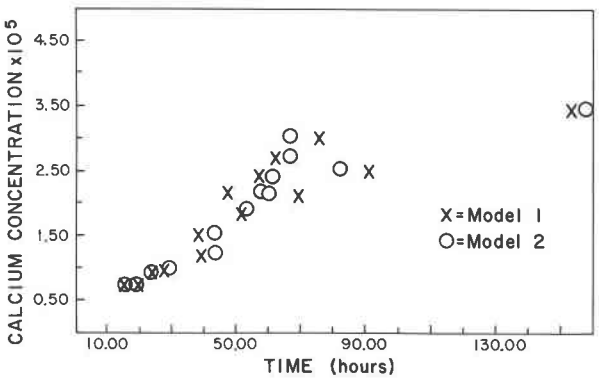

Fig. 5. Concentration of total dissolved calcium as a function of time in a semi-static experiment monitoring dissolution rate of fluorite at 75°C. Data are corrected for dilution by reinjection of fresh solution after each sample using a pseudo-third order rate law, X and a pseudo-zero order rate law, O, as discussed in the Appendix.

These results for fluorite were checked independently by operating the experimental system as a semi-static reactor. In this case, concentrations were monitored as a function of time by periodically withdrawing samples from the autoclaves while simultaneously replacing it with fresh solution. The results (corrected for dilution by the reinjection of fresh solution) are plotted in Figure 5, using two different theoretical rate laws, given in the Appendix. The linearity of this [Ca] vs. time plot again indicates a pseudo-zero order reaction with respect to the calcium in solution far from equilibrium, but pseudo-third order close to equilibrium. Crystals of different sizes were used and the apparent rate of reaction was divided by functions of the surface area. In both the CSTR and in the semi-static experiments, the rate of calcium change was found to be first-order dependent upon the total surface area. Similar

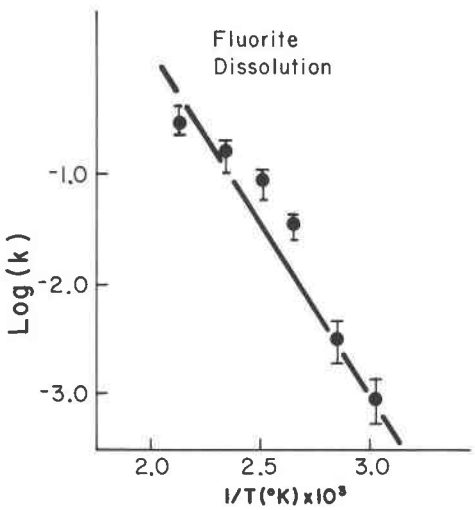

Fig. 6. Arrhenius plot of log (pseudo-zero rate constant, k, far from equilibrium) vs. reciprocal temperature (1/K) for fluorite dissolution in water.

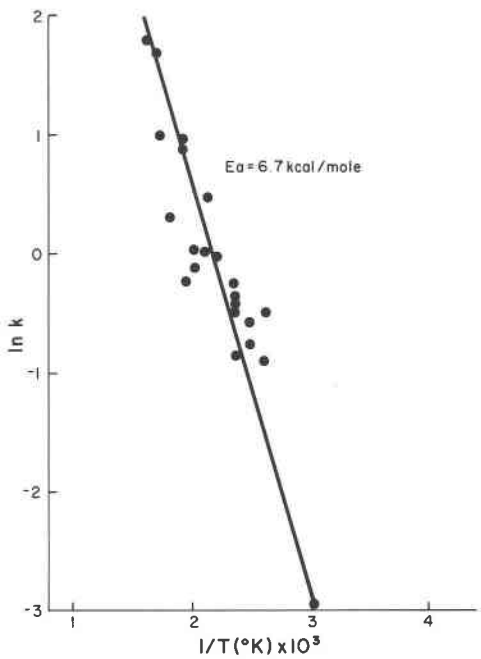

Fig. 7. Arrhenius plot of log (pseudo zero-order rate constant, k, far from equilibrium) vs. reciprocal temperature (1/K) for calcite dissolution in the system $CaCO_3$–H_2O.

experiments were performed using calcite crystals. For brevity, only the Arrhenius plot for calcite is included here.

The Arrhenius activation energies are easily determined by carrying out the experiment in the flow mode at a variety of temperatures. The Arrhenius activation energy, E_a is given by:

$$k = A \exp(-E_a/RT) \text{ or } \ln k = \ln A - E_a/RT \quad (21)$$

where k is the experimental rate constant, R is the universal gas constant, T is the absolute temperature (K), and A is the frequency factor. ln k (pseudo-zero order rate constant) vs. $1/T$ is plotted in Figure 6 for fluorite. Because the plot is linear, the mechanism can be assumed to be the same at all the temperatures for which the experiment was performed. Contrasting with this is the Arrhenius plot for calcite dissolution from our flow data, in Figure 7. The activation energy for calcite dissolution is much less than that for fluorite on the basis of these two curves, as expected from theory. Plots such as these are comparatively easy to collect when operating in the flow mode. To obtain an Arrhenius plot in a static system with eight points would require at least one month of uninterrupted data collection (excluding set-up time, which could boost this by several months). These plots took only 48 hours of uninterrupted data collection. Flow systems of the type described therefore greatly facilitate the collection of kinetic data. However, as mentioned previously, appropriate assumptions must be made concerning the reactor model for the equipment used.

Reactor hydrodynamics assume special significance

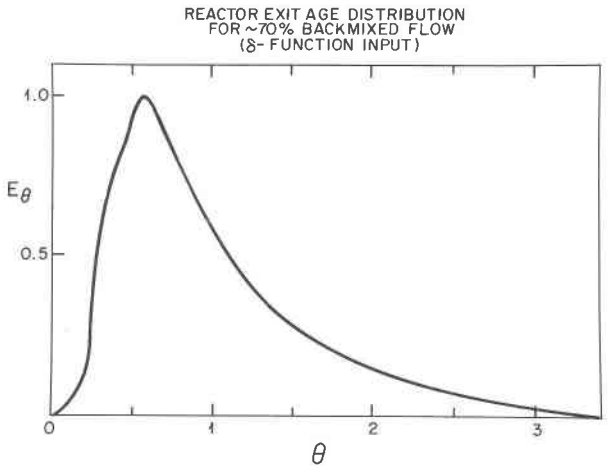

Fig. 8. Tracer concentration in output stream as a function of time for a packed-bed reactor with 70% backmixing. E_θ is (the concentration of the output × void volume)/(volume of the tracer × input concentration). Θ is the residence time.

when consecutive reactions are involved. In natural mineral–water systems, consecutive reactions have not yet been studied extensively, but are of considerable importance. A good example of the effect of reactor backmixing on product distribution is the zeolite-catalyzed conversion of methanol to hydrocarbons in a packed-bed reactor (Chang and Silvestri, 1977; Chang, 1983). This complex consecutive reaction has been found to be representable at sufficiently high temperature by the relatively simple global kinetic model proposed by Chang et al. (1984).

$$A \rightarrow B \rightarrow C \qquad (22)$$

where a = methanol (in equilibrium with dimethyl ether); B = olefins; C = paraffins + aromatics. Backmixing effects will primarily be revealed through changes in the aromatics distribution, due to enhanced contact of A and C resulting in increased ring alkylation by methanol and dimethyl ether. Figure 8 contains the exit age distribution curve from a tracer (δ-function) analysis of a laboratory reactor, showing 70% backmixed flow. This reactor was used for the methanol-to-hydrocarbon reaction. Figure 9 compares the (normalized) aromatics distribution from this backmixed reactor against results from an ideal plug-flow reactor, Figure 10. A shift in the distribution toward higher molecular weight is evident with the backmixed reactor.

The last example demonstrates how to calculate the axial dispersion from inert tracer spikes in tubular reactors. The effluent curve for a δ-function input for a packed-bed (of magnetite) reactor is shown in Figure 11. The reactor had a length of 21 cm, 0.64 cm I.D. and was packed with 50–60 μm diameter magnetite particles. The flow was non-turbulent (Re ≃ 0.01). An axial dispersion parameter (D_a/ul) of 0.0574 was calculated, based on the measured variance of the effluent response curve for the impluse injection of a 0.158 M NaCl solution. Assuming that perfect plug flow exists at the boundaries of the vessel,

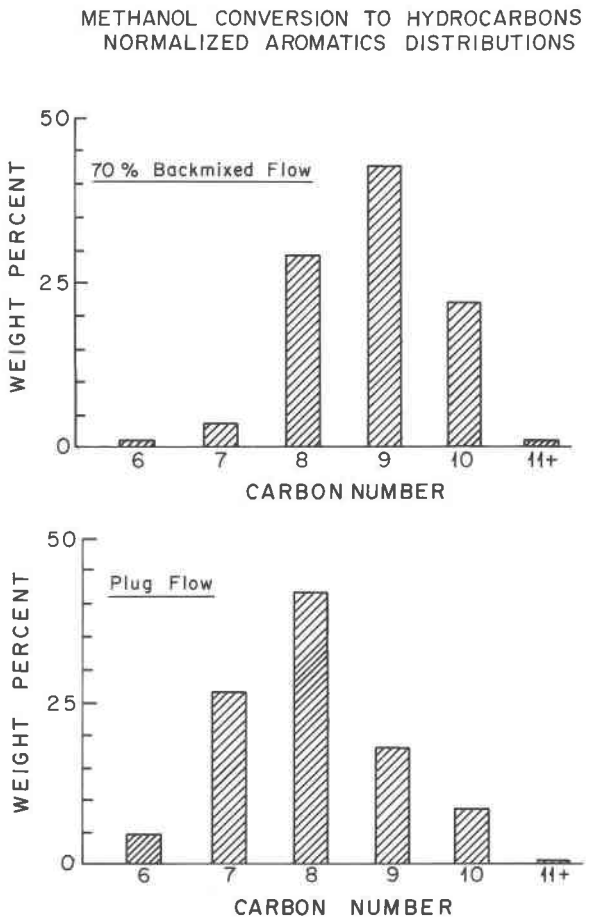

Figs. 9, 10. Comparison of products generated in the zeolite-catalyzed conversion of methanol to hydrocarbons in (9) 70% backmixed and (10) plug-flow, packed bed reactors, respectively. Reaction progress is notably advanced in the backmixed relative to the plug flow reactor.

the following equation (Levenspiel, 1972), yields the axial dispersion parameter:

$$\sigma_\theta^2 = 2x - 2x^2(1 - \exp(-1/x)) \qquad (23)$$

where σ_θ^2 is the variance, θ is the experimentally determined residence time, and x is the axial dispersion parameter, D_a/ul, where u is the superficial velocity and l is the length of the flow tube. Very often the effluent response curve will display a long and extended tail due to the effects of slow moving residual packets of fluid caught in partially stagnant regions within the vessel. Therefore, the data sometimes are truncated at time = 2Θ, to attenuate statistical errors in the calculation.

In summary, we have demonstrated the theory of flow-type experiments and the derivation of kinetic rate laws for use with well-mixed (CSTR) and plug flow regimes. The application of flow type experiments to kinetic studies is illustrated with preliminary data obtained in tubular reactors. Knowledge of the transport and flow dynamics are essential to interpret the kinetic data properly. Failure

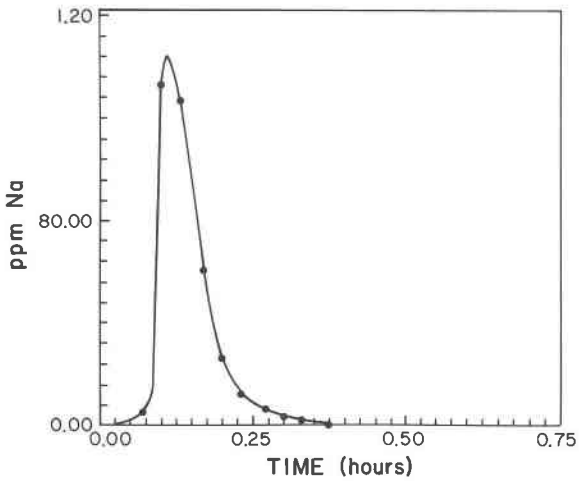

Fig. 11. Experimental tracer curve for a δ-function input of 0.158 M NaCl spike into a packed-bed of magnetite.

to do so can rapidly lead to a vast quantity of misinterpreted data.

Acknowledgments

We thank Maria Borcsik, Don Rimdstidt, Hu Barnes and Mary Barnes for helpful advice on the design of this apparatus. Ted Forseman and Charlie Kulick helped with the final modifications of the design and construction. This work was supported by NSF Grants EAR-82-18726 and CEE-79-20996. Much of this work was made possible by generous support given to D.A.C. by the Shell Companies Foundation.

References

Bunn, R. (1976) Action of Aqueous Alkali on Pyrite. Ph.D. Thesis, Iowa State University.

Carberry, J. (1960) A boundary-layer model of fluid-particle mass transfer in fixed beds. American Institute of Chemical Engineering Journal, 6, 460–463.

Carberry, J. (1976) Chemical and Catalytic Reaction Engineering. McGraw-Hill Book Company, New York.

Chang, C. D. and Silvestri, A. J. (1977) Conversion of methanol and other O-compounds to hydrocarbons. Journal of Catalysis, 47, 249.

Chang, C. D. (1983) Hydrocarbons from Methanol. M. Dekker, New York.

Chang, C. D., Chu, C. T-W., and Socha, R. F. (1984) Methanol conversion to olefins over ZSM-5: 1. Effect of temperature and zeolite SiO_2/Al_2O_3. Journal of Catalysis, 86, 289.

Denbigh, K. G. (1944) Velocity and yield in continuous reaction systems. Transactions of the Faraday Society, 40, 352–373.

Denbigh, K. G., Hicks, M., and Page, F. M. (1947) Kinetics of open reaction systems. Transactions of the Faraday Society, 41, 479–494.

Frank-Kamenetskii, J. (1955) Diffusion and heat exchange in chemical kinetics. Plenum Press, New York, Chapters 1–5.

Hill, C. G., Jr. (1977) An Introduction to Chemical Engineering Kinetics and Reactor Design. John Wiley and Sons, New York.

Johnson, A. I. and Huang, C. (1956) Mass transfer studies in an agitated vessel. American Institute of Chemical Engineers Journal, 2, 412–419.

Kanert, G. A., Gray, G. W., and Baldwin, W. G. (1978) The solubility of magnetite in basic solutions at elevated temperatures. Atomic Energy of Canada Limited (Whiteshell Nuclear Research Establishment) AECL-5528.

Lagache, M. (1976) New data on the kinetics of the dissolution of alkali feldspars at 200°C and CO_2 charged water. Geochimica et Cosmochimica Acta, 40, 157–161.

Laidler, K. J. (1965) Chemical Kinetics, 2nd Ed. McGraw-Hill, Inc., New York.

Lasaga, A. T. and Kirkpatrick, R. (1981) Kinetics of Geochemical Processes. Reviews in Mineralogy, Volume 8. Mineralogical Society of America, Washington, D.C.

Levenspiel, O. (1972) Chemical Reaction Engineering. John Wiley and Sons, New York.

Levenspiel, O. and Bischoff, K. B. (1963) Patterns of flow in chemical process vessels. Advances in Chemical Engineering, 4, 95–197.

Morey, G. W. and Hesselgesser, J. M. (1951) The solubility of some minerals in superheated steam at high pressures. Economic Geology, 46, 821–835.

Poirier, R. V. and Carr, R. W. (1971) Use of tubular flow reactors for kinetic studies over extended pressure ranges. Journal of Physical Chemistry, 75, 1593–1600.

Rimstidt, J. D. and Barnes, H. L. (1980) The kinetics of silica–water reactions. Geochimica et Cosmochimica Acta, 44, 1683–1699.

Sherwood, R. T., Pigford, R. L., and Wilke, C. R. (1975) Mass Transfer. McGraw-Hill Chemical Engineering Series, New York.

Sweeton, F. H. and Baes, C. F. (1970) The solubility of magnetite and hydrolysis of ferrous ion in aqueous solutions at elevated temperatures. Journal of Chemical Thermodynamics, 2, 479–500.

Tremaine, P. R. and LeBlanc, J. C. (1980) The solubility of magnetite and the hydrolysis of Fe^{2+} in water to 300°C. Journal of Solution Chemistry, 9, 415–442.

Wilson, E. J. and Geankoplis, C. J. (1966) Liquid mass transfer at very low Reynolds numbers in packed beds. Industrial and Engineering Chemistry Fundamentals, 5, 9–14.

Zahner, J. C. (1972) Experimental study of laboratory flow reactors. Advances in Chemistry Series (American Chemical Society), 109, 210.

Manuscript received, October 23, 1984;
accepted for publication, September 22, 1985.

Appendix

One must smooth discontinuous data in order to correct for the dilution while sampling in the semi-static mode. The method is given below and makes the following assumptions. (1) Ratio of surface area to mass of water in the vessel is constant throughout the course of the experiment. (2) Concentration change with respect to time can be expressed as a simple integratable function. (3) No mixing occurs while simultaneously replacing fluid. However, immediately after fluid is replaced, mixing is instantaneous. (4) A function $dc/dt = f'(c, t)$ is initially assumed and the integrated form of this expression is used in the method below. The best straight line obtained using the integrated rate law, is assumed to be the proper rate expression.

In general, if $f(c) = kt$ then at $t = 1$, $f(c_1) = k_1$ or $f(c_i) = k_i$, where $f(c)$ is the integrated form of the test rate law. At the ith sampling, the volume of fluid is replaced with the same volume of pure water, thus diluting the concentration in the vessel to a new concentration, C_{Ni}. If M is the total mass of fluid contained in the vessel and m, the sampling mass, then the new molal concentration, C_{Ni} is:

$$(M - m)C_i/M = C_{Ni} \qquad \text{A1}$$

This is assumed to have the effect of decreasing the real time axis. In calculating the corrected time, the new concentration is used. t_{Ni} is the new time, when $C(t) = C_{Ni}$.

$$f(C_{Ni})/k_i = t_{Ni} \qquad \text{A2}$$

Thus, the corrected real time for the i + 1 sample can be given by:

$$t_{Ri+1} = t_{i+1} \quad \text{A3}$$

where t is the actual laboratory time, and t_R is the corrected time.

Theoretical example

Letting f(c) = c, k = 3 or c = 3t, the following data would result if no dilution were made. Data are given as (t, c). (0, 0.00); (1, 3.00); (3, 9.00); (4, 12.00); (5, 15.00); and (6, 18.00). However, if 1 mL is removed and replaced in a volume of 10 mL, the following points result, given as (t, c): (0, 0.00); (1, 3.00); (2, 5.70); (3, 8.13); (4, 10.30); (6, 15.29).

Step 1
Try c = kt, and calculate k_i.
$C_1 = 3$; $t_1 = 1$; and $k_1 = 3$.
Step 2
Calculate C_{N1}.
3(9/10) = 2.7, from equation A1.
Step 3
Calculate t_{N2}.
$C_{N1}/K_1 = t_{N1}$ or 2.7/3.0 = 0.9.
Step 4
Calculate t_{R2}.
$t_{R2} = t_2 - t_1 + t_{N1}$
$2 - 1 + 0.9 = 1.9 = t_{R2}$.
Step 5
Check C_2 at R_2.
C_2 calculated = 5.70.

Continue in the same manner for the remainder of the data. The corrected data should be (t_{Ri}, C_i): (0.00, 0.00); (1.00, 3.00); (1.90, 5.70); (2.71, 8.13); (3.43, 10.30); (5.10, 15.29). This yields equivalent data to the undiluted case.

In Figure 5, two rate expressions were tried in determining the proper rate expression, a pseudo-zero order rate law, and a pseudo-third order rate law with respect to calcium. If CaF_2 dissolves congruently, and the rate of dissolution is proportional to the degree of displacement from equilibrium, then:

$$K_e = [Ca^{2+}]_e[F^-]_e^2 \quad \text{A4}$$

Table A1.

( ) indicates calculated data based on the trial rate law, no experimental starting point.

Lab Time	Concentration (Calcium)	Zero order, O Method 2	Third order, X Method 1
Hours		Hours	Hours
24.0	9.0×10^{-6}	24.0	24.0
	(7.2×10^{-6})	(19.2)	(15.2)
48.0	1.2×10^{-5}	43.2	39.2
	(9.6×10^{-6})	(28.6)	(27.3)
72.0	1.85×10^{-5}	52.6	51.3
	(1.5×10^{-5})	(43.0)	(38.0)
96.0	2.7×10^{-5}	67.0	62.0
	(2.2×10^{-5})	(58.4)	(47.2)
120.0	2.5×10^{-5}	82.4	91.2
	(2.0×10^{-5})	(59.7)	(69.1)
126.5	3.0×10^{-5}	66.2	69.1
	(2.4×10^{-5})	(61.5)	(57.3)
222.5	3.45×10^{-5}	157.5	153.3

where K_e is the equilibrium solubility product. If $[Ca^{2+}] = [F^-]/2$, then $4[Ca^{2+}]^2 = [F^-]^2$ for stoichiometric dissolution in pure water. Therefore,

$$K_e - [Ca^{2+}][F^-]^2 = K_e - 4[Ca^{2+}]^3 \quad \text{A5}$$

where $[Ca^{2+}]$ is the molal concentration measured. The raw data and calculated data are given in the tabulation. The parentheses indicate calculated concentrations and times for that concentration, according to the rate law assumed. Note: the pseudo-zero and -third order rate forms yield virtually the same results far from equilibrium, as expected. However, close to equilibrium, of these two trial rate expressions, only the integrated form of the pseudo-third order rate law is linear.